JOURNAL OF CATALYSIS **179,** 581–596 (1998)
ARTICLE NO. CA982251

# FT-IR Studies on Light Olefin Skeletal Isomerization Catalysis

## III. Surface Acidity and Activity of Amorphous and Crystalline Catalysts Belonging to the $SiO_2$–$Al_2O_3$ System

Marcella Trombetta,* Guido Busca,* Stefano Rossini,† Valerio Piccoli,† Ugo Cornaro,† Alberto Guercio,† Roberto Catani,† and Ronald J. Willey‡

*Istituto di Chimica, Facoltà di Ingegneria, Università, P.le J.F. Kennedy, I-16129 Genoa, Italy; †Snamprogetti, via Maritano 26, I-20097 San Donato Milanese, Milan, Italy; and ‡Department of Chemical Engineering, Northeastern University, Boston, Massachusetts 02115
E-mail: icibusca@csita.unige.it; stefano.rossini@snamprogetti.eni.it; willey@neu.edu

Received March 12, 1998; revised July 13, 1998; accepted July 21, 1998

**The surface acidity of both amorphous and crystalline materials belonging to the $SiO_2$–$Al_2O_3$ system (i.e., amorphous silicas, amorphous silica–aluminas with different Al contents, HZSM5 and H-ferrierite (FER) zeolites, and silicated and pure $\gamma$-$Al_2O_3$) have been studied using the FT-IR spectroscopy of the surface hydroxy groups and of adsorbed acetonitrile (AN) and pyridine (Py). Lewis bonded and H-bonded species of AN have been observed, while a protonated form of adsorbed AN has been characterized on HZSM5. A molecular sieve effect has been found for Py adsorption on FER and HZSM5. The catalytic activity of these materials in the skeletal isomerization of 1-butene to isobutene has also been investigated. The Brønsted surface acidity scale found correlates well with the catalytic activity in 1-butene conversion, measured after 20–40 min time on stream. The selectivity to isobutene follows nearly an inverse trend, except for FER, which shows both higher activity and higher selectivity than silica–alumina, quite good resistance to coking, and selectivity increasing with time on stream. Comparative analysis of the behavior of these catalysts and of the spectrum of their surface OH groups gives new light on the structure of the acidic OHs on materials belonging to the $SiO_2$–$Al_2O_3$ system. The usefulness of zeolite and alumina-based catalysts for skeletal isomerization of *n*-butene to isobutene is also briefly discussed.** 

### INTRODUCTION

The skeletal isomerization of *n*-butene to isobutene and of *n*-pentene to isoamylene are topics of increasing interest (1, 2) because of the demand for isoolefins in relation to the increasing request for branched ethers (MTBE, ETBE, and TAME) for reformulated gasoline (3). Two main catalyst types have been proposed for this reaction: those based on aluminas (chlorided (4, 5), silicated (6, 7), and borated $Al_2O_3$ (8, 9)) and those based on protonic zeolites. Among zeolites, ferrierite (10, 11) was reported to be a unique catalytic material for the conversion of *n*-butene to isobutene. Other acid catalysts such as HZSM5 zeolite and silica–aluminas are also active for this reaction, although selectivity is quite low due to the concurrence of oligomerization, transmutation, disproportionation, and aromatization reactions (1, 2). On the other hand, all catalysts tend to deactivate by coking and need more or less frequent reactivation treatments. Thus, the rate of deactivation and the stability upon multiple activity/reactivation cycles are also factors affecting long-term catalyst performance.

Most authors believe that this reaction is catalyzed by protonic acids (12–14). However, the relations between the catalyst's activity and selectivity and the strength (15) and density (16) of the Brønsted acid sites and the shape selectivity effect (9, 17–21) are still imperfectly known or under debate. Other authors, in contrast, support the idea that Lewis sites can act in this reaction (22), and discussion still exist on the role of carbonaceous materials and of dimeric intermediates (23, 24).

In a systematic investigation of the chemical features of this reaction (7, 9, 25, 26) we studied several different catalysts, both crystalline and amorphous, belonging to the $SiO_2$–$Al_2O_3$ system. In this paper we report an attempt to relate the surface acidity of these strongly related catalytic materials, as observed by FT-IR spectroscopy, with their activity in the *n*-butene to isobutene isomerization reaction.

### EXPERIMENTAL

Data on some of the catalyst samples under study are summarized in Table 1. Some catalytic materials are commercial. Some silica and silica–alumina samples with variable Al content are aerogels, prepared with a supercritical drying procedure closely similar to that described previously (27). Silicas and silica–aluminas are amorphous to XRD analysis. The ferrierite sample (Si/Al atomic ratio = 20) has been prepared following a procedure from the literature (10). XRD and skeletal FT-IR data show that it is well crystallized, without any observable impurity. Previous to catalytic runs this sample was calcined at 823 K.



0021-9517/98 $25.00

**TABLE 1**

**Characteristics of the Catalysts under Study**

| Samples | Notation | Si/Al atomic ratio | Origin | Surface area $m^2/g$ |
|---|---|---|---|---|
| Pure silica | S1 | ∞ | Fluka | 750 |
| Pure silica | S2 | ∞ | Aerogel | 870 |
| Silica–alumina | SA8 | 9.2 | Aerogel | 220 |
| Silica–alumina | SA13 | 5.8 | Strem | 330 |
| Silicated alumina | AS | 0.02 | Snamprogetti | 190 |
| Pure alumina | A | 0 | Akzo | 190 |

The HZSM5 sample was from Engelhard (Si/Al atomic ratio = 23).

The IR spectra were recorded on a Nicolet Magna 750 Fourier transform instrument, using pressed disks of pure catalyst powders, activated by outgassing at 773 K into the IR cell.

The catalytic tests reported here were performed with 1-butene at 0.8 Atm (81.04 kPa, dilution with isobutane) under the conditions reported in Table 2 with a fixed-bed tubular reactor (internal diameter 12 mm, with a coaxial internal thermocouple with 5 mm external diameter). The catalyst granulometry was 20–25 mesh. The products were recovered integrally for either 20 or 40 min on stream and were analyzed by on-line gas chromatography (HP 5890) using a FID detector and a 50 m Chrompack PLOT $Al_2O_3/Na_2SO_4$ capillary column for 1-butene/isobutene separation and a 50 m PONA capillary column for the analysis of all other products.

## RESULTS

### *(a) Catalytic Activity*

The catalytic activities of some of the samples under study are summarized in Table 2. They have been measured under conditions similar to those for an industrial process with catalysts based on aluminas (6–9). All catalysts deactivate more or less rapidly upon stream. To have homogeneous data, the products are integrally recovered in a time on stream range between $t_1$ and $t_2$: $\Delta t = t_2 - t_1$ is generally 20 min after at least 15 or 20 min time on stream. Selectivity to coke did not exceed 1% in all cases.

Alumina is quite an active catalyst for *n*-butene conversion at 743 K and is highly selective for isobutene synthesis, as already shown (1, 5, 7, 26). As already discussed (26), *n*-butenes are in thermodynamic equilibrium, while the isobutene amount is definitely lower than that possible in thermodynamic equilibrium (28). The main side reactions give rise to $C_3$ and $C_5$ hydrocarbons (mainly propene and isopentenes, with significant amounts of *n*-pentene too), $C_4$ paraffins, and $C_8$ aromatics. According to our previous studies, we concluded that the "monomolecular" skeletal isomerization of *n*-butenes is competitive with its dimerization to $C_8$ compounds that give rise to $C_3 + C_5$ olefins by cracking. Other by-reactions give rise mainly to $C_8$ aromatics and

**TABLE 2**

***n*-Butene Conversion Data on Various Catalysts Belonging to the $SiO_2$–$Al_2O_3$ System**

| Catal. | $W_{cat}$ g | LHSV $h^{-1}$ [a] | $T$ K | $P_{1\text{-}C4H8}$ atm[b] | $t_1$ min[c] | $t_2$ min[c] | Conv. % | $S_{iso}$ % | $S_{C1-C3}$ % | $S_{C3=}$ % | $S_{C4sat}$ % | $S_{C5}$ % | $S_{arom}$ %[d] | $S_{C6+}$ %[e] |
|---|---|---|---|---|---|---|---|---|---|---|---|---|---|---|
| A | 1.5 | 4.4 | 743 | 0.8 | 20 | 40 | 34.8 | 71.0 | 6.9 | 6.5 | 0.8 | 13.1 | 1.2 | 7 |
| | 1.5 | 10.2 | 753 | 0.8 | 20 | 40 | 34.6 | 80.0 | 4.7 | 4.4 | 0.7 | 8.8 | 1.1 | 4.7 |
| AS | 1.5 | 4.4 | 743 | 0.8 | 20 | 40 | 43.5 | 75.5 | 5.0 | 4.9 | 0.9 | 12.1 | 1.5 | 5 |
| SA13 | 1 | 4.5 | 703 | 0.8 | 15 | 45 | 40.5 | 27.9 | 15.8 | 15.2 | 12.5 | 24.7 | 2.1 | 17 |
| | 1 | 8.4 | 703 | 0.8 | 20 | 40 | 31.4 | 29.6 | 15.6 | 15.0 | 9.8 | 24.6 | 1.1 | 19.3 |
| | 1.2 | 10.1 | 703 | 0.8 | 20 | 40 | 28.7 | 30.1 | 14.8 | 14.6 | 7.8 | 24.0 | 1.0 | 22.3 |
| | 1 | 4.8 | 723 | 0.8 | 15 | 45 | 42.5 | 28.6 | 17.0 | 16.2 | 10.8 | 25.5 | 1.4 | 16.7 |
| | 1 | 7.6 | 723 | 0.8 | 20 | 40 | 34.6 | 30.3 | 16.0 | 15.8 | 9.1 | 25.2 | 1.3 | 18.1 |
| | 1 | 11.5 | 723 | 0.8 | 20 | 40 | 28.5 | 31.6 | 15.5 | 15.2 | 8.1 | 24.6 | 1.2 | 19 |
| FER | 0.5 | 6.0 | 703 | 0.8 | 20 | 40 | 55.4 | 62.4 | 11.2 | 9.6 | 3.4 | 10.2 | 1.1 | 11.7 |
| | 0.5 | 6.0 | 703 | 0.8 | 1435 | 1455 | 36.9 | 88.0 | 1.6 | 1.5 | 1.1 | 1.9 | 0.3 | 7.1 |
| | 0.5 | 8.7 | 723 | 0.8 | 20 | 40 | 45.2 | 78.1 | 5.4 | 4.6 | 2.9 | 4.2 | 0.2 | 9.2 |
| HZSM5 | 0.6 | 20.3 | 733 | 0.8 | 20 | 40 | 87.8 | 10.4 | 24.4 | 18.3 | 11.6 | 17.7 | 3.6 | 32.3 |
| | 0.6 | 23.6 | 723 | 0.8 | 20 | 40 | 84.5 | 13.1 | 16.4 | 13.6 | 8.3 | 23.2 | 2.7 | 36.3 |
| | 0.6 | 27.3 | 723 | 0.8 | 220 | 260 | 84.3 | 13.6 | 20.7 | 16.9 | 6.5 | 23.1 | 2.1 | 34 |
| | 1.0 | 11.4 | 703 | 0.8 | 20 | 40 | 98.1 | 1.6 | 19.0 | 0.5 | 19.3 | 12.5 | 11.9 | 35.7 |
| | 1.1 | 8.9 | 703 | 0.8 | 20 | 40 | 98.6 | 1.4 | 20.5 | 0.8 | 20.1 | 14.5 | 13.6 | 29.9 |

[a] LHSV = liquid hourly space velocity (liquid feed density = 0.6 g/ml).
[b] $P_{tot} = 1$ atm; dilution with isobutane.
[c] $t_1$ and $t_2$ are the times on stream of starting and stopping product collection, respectively.
[d] All aromatics, but maily C8 aromatics.
[e] Nonaromatic hydrocarbons.

to $C_4$ paraffins. The catalyst cokes progressively, probably primarily due to higher oligomer formation.

Silication of alumina definitely increases the activity and also improves the selectivity to isobutene a little. In the best conditions, selectivities higher than 80% at near 37% conversion can be obtained over silicated alumina.

Silica–alumina is definitely more active than both pure and silicated alumina. In fact, the same conversion levels are attained at significantly lower temperatures. However, the selectivity to isobutene at the same conversion level is much smaller. Cracking of dimers to $C_3 + C_5$ compounds is apparently the main by-reaction, but hydrogenation to saturated butanes is also quite important. Instead, selectivity to aromatics is similar to that on alumina. By increasing the space velocity the *n*-butene conversion decreases, as expected, but selectivity to isobutene is increased only a little. Interestingly, isobutene selectivity increases also by increasing reaction temperature, while selectivity to $C_3$ and $C_5$ compounds decreases. This further supports the idea that $C_3$ and $C_5$ products mainly arise from cracking of $C_8$ dimeric compounds, dimerization being unfavored by increasing temperature.

FER is even more active than silica–alumina. Conversion is definitely higher at the same temperature. However, selectivity to isobutene is much higher than on silica–alumina although, for fresh catalysts, it is only slightly better than for silicated alumina in comparable conditions. As already shown (10, 11, 20), a main characteristic of this catalyst is, among the more active ones, to retain significant activity and to increase its selectivity strongly with time on stream. In fact, as shown in Table 2, after 1435 min conversion is still quite high and selectivity increased (up to 88%). In these conditions, all by-reactions are definitely slowed down more than the skeletal isomerization.

The catalytic activity of HZSM5 zeolite is far higher with respect to all other materials investigated here, but with far lower selectivities to isobutene and great production of all byproducts except propene. Aromatics are also produced in large amounts. By strongly increasing the space velocity conversion decreases to near 85% but selectivities to isobutene do not grow so much (<14%). Isobutene yield no higher than 20% can be obtained with this material. These data again agree with the literature (1, 19, 20, 29).

As is well known, a debate is still occurring on the possible role of dimeric $C_8$ species as intermediates in skeletal isomerization on FER and other catalysts. To evaluate this point, we have plotted the curves of selectivity to isobutene and to $C_8$ species vs conversion on both FER and silicated alumina (Fig. 1) and extrapolated them as conversion $\rightarrow 0$. These plots suggest that both isobutene and $C_8$ species are primary products.

*(b) FT-IR Spectra of the Catalyst's Hydroxy Groups*

In Fig. 2 the spectra of the surface hydroxy groups of the catalysts, previously activated by outgassing at 873 K,

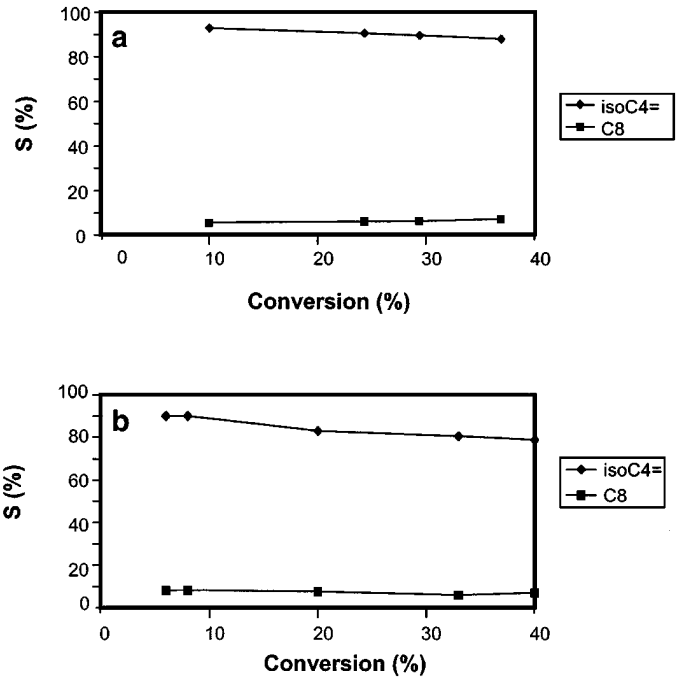


**FIG. 1.** Selectivity vs conversion for FER (a) and silicated alumina (b) catalysts.

are shown. The spectra of pure silica samples (Fig. 2g) are just coincident, showing a single sharp band at 3745 $cm^{-1}$, in agreement with a number of previous data, as reviewed some years ago (30, 31). This band is certainly dominated by the absorption due to the O–H stretching mode of a single terminal Si–OH group (Scheme 1, Species I), although it is agreed today that it also contains the O–H stretchings

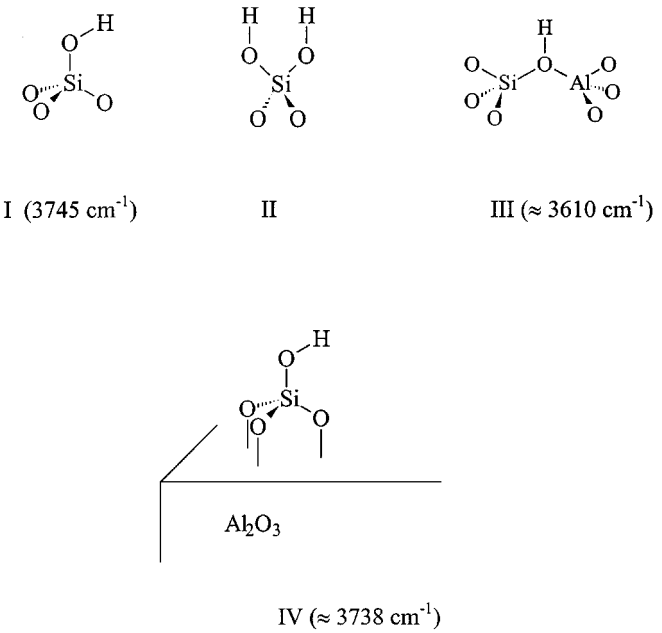


**SCHEME 1**

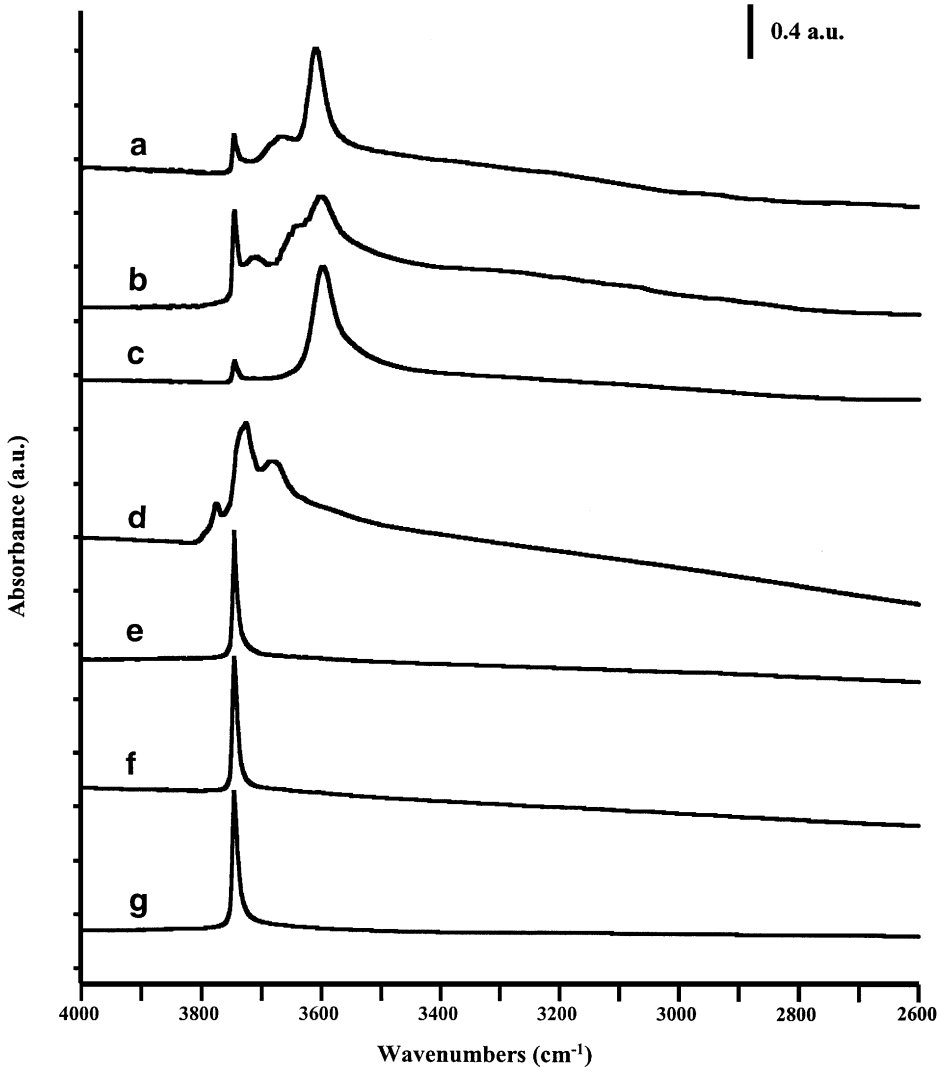


**FIG. 2.** FT-IR spectra of the catalysts HZSM5 (a), FER1 (b), FER2 (c), AS (d), SA13 (e), SA8 (f), S2 (g) in the O-H stretching region after outgassing at 873 K.

of geminal silanols (Scheme 1, Species II) (32, 33) and of weakly perturbed vicinal pairs of terminal silanols (34), both contributing to the tail at the low-frequency side of the main band.

The spectra of the silica–alumina samples (Figs. 2e and 2f) are, in these conditions, absolutely indistinguishable from those of the pure silica samples. They also present a single band at 3745 $cm^{-1}$, in agreement with most literature data (30, 31).

It seems obvious to assign the bands at ca. 3745 $cm^{-1}$ observed in the spectra of silica–alumina samples to the same species as those observed on pure silica, due to the absolute similarity of the spectra, and to their absorption region, considered to be typical for terminal OHs (30). However, in the literature a different species, i.e., a bridging hydroxide between an Al and a Si atom (Scheme 1, Species III), is assumed (30, 31, 35, 36) to exist on silica–alumina and to be responsible for strong Brønsted acidity. This will be further discussed below.

The spectrum of the silicated alumina sample (Fig. 2d) is more complex. As discussed previously (7), it is dominated by the spectrum of the surface OHs of alumina (7, 26, 30, 31, 37, 38), with bands near 3790 (shoulder), 3770, 3730, and 3680 $cm^{-1}$, with an additional shoulder observed near 3738 $cm^{-1}$. This new band, made more evident after subtraction of the spectrum of the OHs of alumina (7), has been assigned by us to a silanol group such as Species I (Scheme 1), but anchored on the surface of alumina (Scheme 1, Species IV). The lowering of the O–H stretching frequency from 3745 to 3738 $cm^{-1}$ for silicated alumina with respect to silica or silica–aluminas agrees with that previously found for silicated titania (39) and can be assigned to the formation of three bonds from the hydrogen-orthosilicate species H–O–$SiO_3$ with Al (and Ti) cations. Such bonds are more

ionic than those with other Si atoms, which are nearly covalent, so that the electron density at Si can be enhanced.

The spectrum of the HZSM5 zeolite (Fig. 2a) agrees with those reported previously for the same catalyst (40–42). It shows a weak sharp maximum at 3747 $cm^{-1}$, with a shoulder at lower frequency (3730 $cm^{-1}$), a broad band with components at 3690 and 3677 $cm^{-1}$, and, finally, a very intense band at 3612 $cm^{-1}$. According to the literature, the stronger band is associated with the strongly Brønsted acidic OHs of the HZSM5 zeolite, which is usually depicted as type III of Scheme 1 (30, 31, 43–45), located in the zeolite cavities. The weaker band at 3747 $cm^{-1}$ is usually assigned to nonacidic silanol groups (Scheme 1, type I) related to Al-free silicalite-type grains, exposed at the external surface. The weak component at 3730 $cm^{-1}$ is likely associated with nonacidic silanols located in internal pores like those of silicalite (46). Finally, the broad band in the 3700–3650 $cm^{-1}$ region is due to the OHs of extra-framework alumina. These data and the relative intensity of the above $\nu$OH bands characterize our sample as a typical HZSM5 zeolite with high Al content and with significant amounts of extraframework alumina.

Two main bands also characterize the spectrum of the ferrierite sample used in catalysis (FER1, Fig. 2b), one quite broad centered at 3602 $cm^{-1}$ and the other, very sharp, detected at 3746 $cm^{-1}$. However, we also detect additional quite broad components near 3710 and 3650 $cm^{-1}$. The literature data concerning the surface OHs of ferrierite are few and disagree in part with each other. All papers agree on the location of the main IR band assigned to the "zeolitic" bridging hydroxy group (Scheme 1, type III) near 3600 $cm^{-1}$, i.e., slightly shifted to lower frequencies with respect to HZSM5 (3610–3620 $cm^{-1}$). An exception is the review of Jacobs (47) that places this band at higher frequency for ferrierite than that for HZSM5 (MFI). All authors also agree on the presence of the band of terminal silanols (Scheme 1, type I, ca. 3745 $cm^{-1}$). In contrast, while the spectra reported by Naber *et al.* (48) and by Wichterlovà (49) only present such two bands, Jin *et al.* (50) show for one of their samples additional bands at 3660 and 3645 $cm^{-1}$, and Komarov and Malachevich (51) observed additional bands at 3660, 3620, and 3560 $cm^{-1}$.

To have information on the nature of the additional bands we found, we also recorded the spectrum of a sample previously calcined at 573 K only. It actually only shows the bands at 3746 and 3602 $cm^{-1}$ (FER2, Fig. 2c). We concluded that the additional bands found in the catalyst calcined at 823 K, used in catalytic experiments, are due to nonframework species arising by the partial collapse of the structure.

### *(c) Interaction of Acetonitrile (AN) with the Surface Hydroxy Groups*

The spectra of the surface hydroxy groups of the different catalysts in contact with acetonitrile (AN) vapor, used as a weak basic probe, are shown in Fig. 3, while those recorded after following outgassing at r.t. are shown in Fig. 4.

In the case of pure silica we detect, in the presence of the vapor (Fig. 3f), a strong broad but very symmetric band centered at 3415 $cm^{-1}$ certainly formed at the expense of the band of the free hydroxyls at 3745 $cm^{-1}$. The shift we measure upon adsorption ($\Delta\nu$ = ca. 330 $cm^{-1}$) is similar to that reported in the literature (52, 53). This band can reasonably be assigned to the H-bonded species reported in Scheme 2 (species I-AN).

The spectrum of the activated silica sample is quickly restored by outgassing at r.t. (Fig. 4f) showing that H-bonding of AN with Species I (Scheme 2) hydroxyls is quite weak.

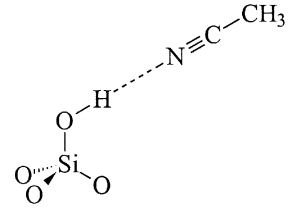


I-AN


III

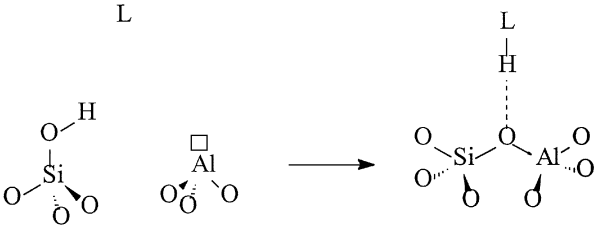


I'

**SCHEME 2**

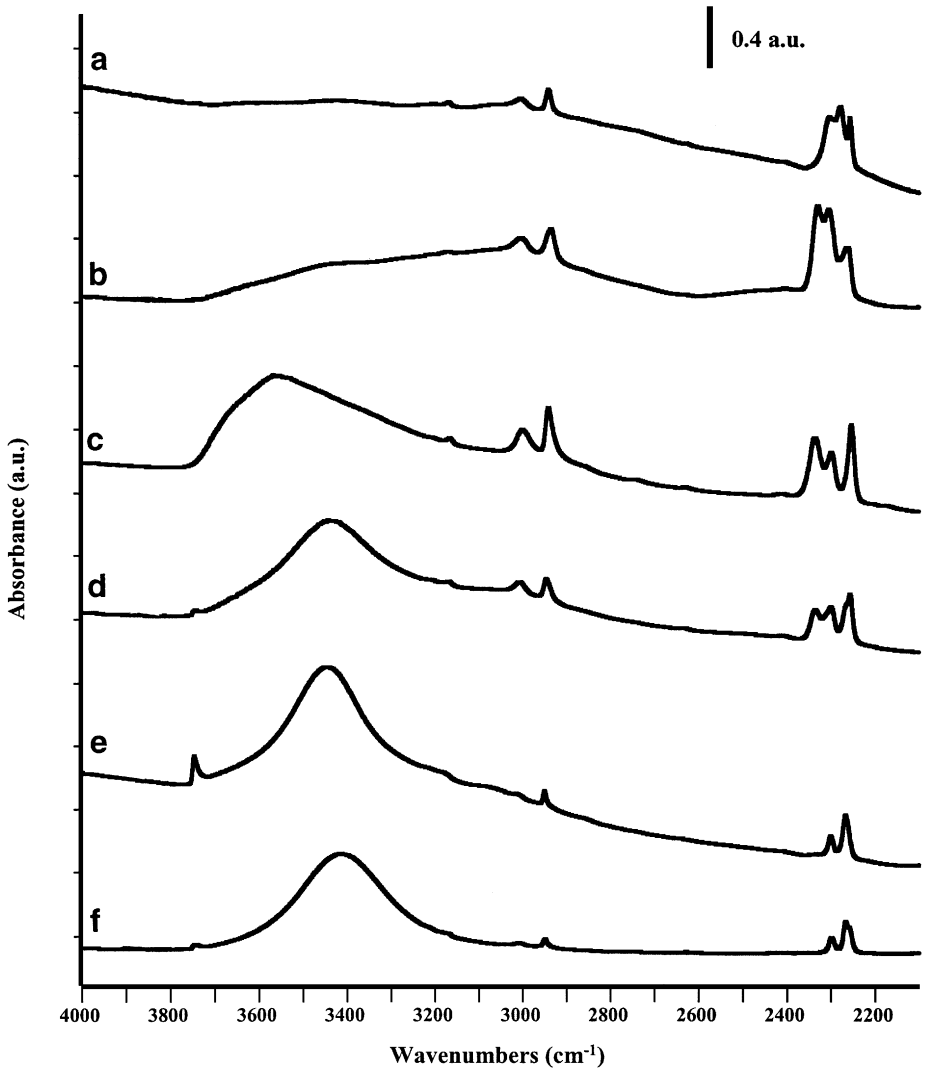


**FIG. 3.** FT-IR spectra (4000–2100 $cm^{-1}$) of the catalysts HZSM5 (a), FER1 (b), AS (c), SA13 (d), SA8 (e), S2 (f) at 300 K in contact with acetonitrile vapour (10 Torr).

The spectrum observed on silica–aluminas is different. In this case in fact, a predominant quite broad band is observed, but in this case it is centered at $3448 \pm 5$ $cm^{-1}$ ($\Delta\nu =$ ca. 300 $cm^{-1}$), i.e., is definitely located at higher frequencies than for silica. On the other hand, a broad tail is also evident at the lower frequency side of this band (centered near 2950 $cm^{-1}$, partly superimposed on the sharp bands near 3000 and 2940 $cm^{-1}$, due to C-H stretchings of AN), and it seems to grow with increasing Al content. Thus, a species with a very high O-H frequency shift ($\Delta\nu =$ ca. 800 $cm^{-1}$) is also formed. This datum confirms the previous one of Sempels and Rouxhet (54). These authors, who found in the spectrum of activated silica–alumina samples only the band at ca. 3745 $cm^{-1}$, concluded that two different hydroxy groups give rise to a single O-H stretching on clean silica–alumina but to two different H-bonding species with AN and other bases (55). In the case of the interaction of AN with silica alumina cracking catalyst (Fig. 3e), we find also a component, very broad, centered near 2350 $cm^{-1}$ (superimposed on the CN stretching bands that will be discussed below).

Outgassing does not completely restore the spectrum of the activated sample, at least in the case of the cracking catalyst SA13 (Fig. 4d), which still contains features due to adsorbed AN and a weak and very broad feature extending between 3600–2000 $cm^{-1}$ with an apparent maximum still near 2950 $cm^{-1}$ ($\Delta\nu =$ ca. 800 $cm^{-1}$). It is consequently believed that another adsorbed species, different from I-AN (Scheme 2), is formed and involves silanol groups somehow different from I or II (Scheme 1).

In the case of silicated alumina, AS, the spectrum recorded in the presence of the gas (Fig. 3c) shows that all hydroxy groups are more or less perturbed as a result of the adsorption of AN. However, subtraction spectra (Fig. 5)

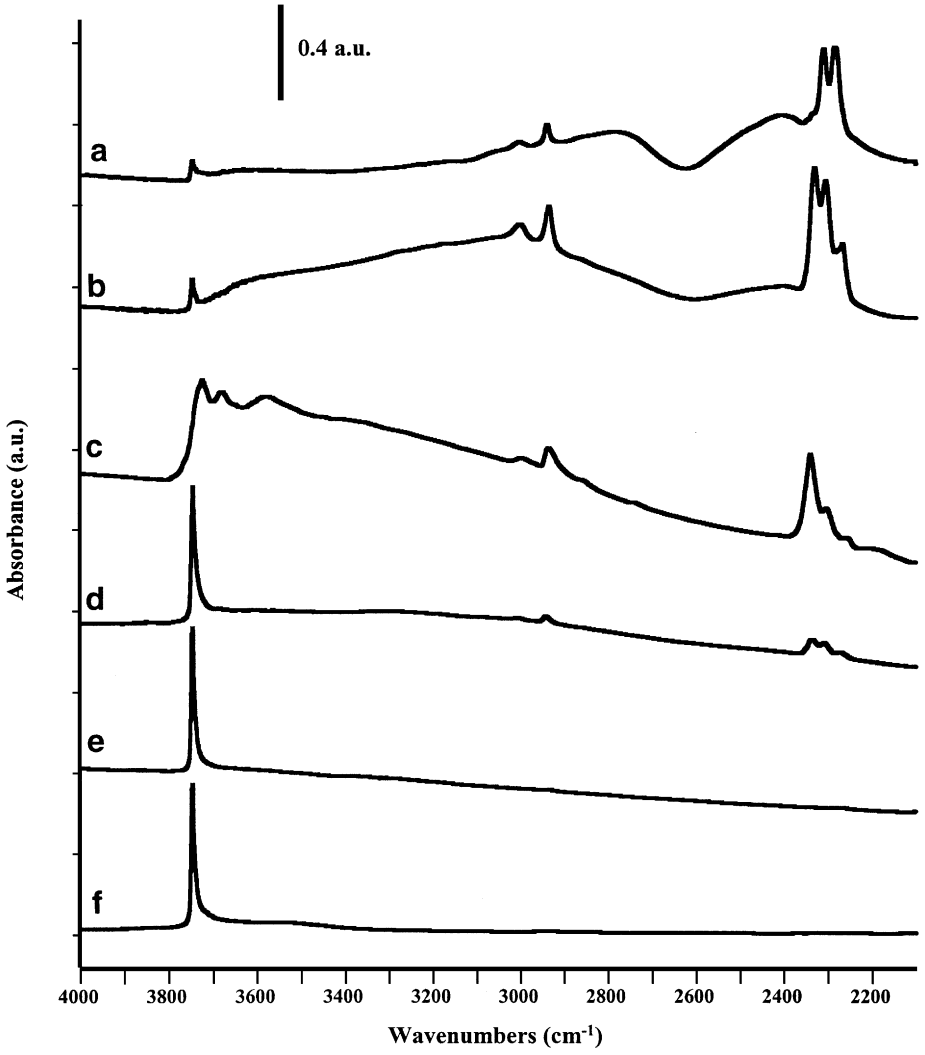


**FIG. 4.** FT-IR spectra (4000–2100 $cm^{-1}$) of the catalysts HZSM5 (a), FER1 (b), AS (c), SA13 (d), SA8 (e), S2 (f) after acetonitrile adsorption at 300 K and successive outgassing at 300 K.

show that the OH responsible for the band near 3735 $cm^{-1}$ (i.e., that assigned to the terminal silanol type IV, Scheme 1) is the most involved in reversible H-bonding, with a shift to near 3540 $cm^{-1}$ ($\Delta\nu$ = ca. 200 $cm^{-1}$). However, the shape of the band is clearly asymmetric and shows an unresolved component centered near 3300 $cm^{-1}$ ($\Delta\nu$ = ca. 450 $cm^{-1}$). This suggests that, while most type IV silanols (Scheme 1) are less acidic than those of silica, some of them have a slightly higher acidity.

In the case of FER in contact with AN vapor (Fig. 3b) the band in the region 3450–3400 $cm^{-1}$ is present only as a broad shoulder. The spectrum is dominated by the features near 2950 and 2350 $cm^{-1}$, i.e., similar to but far more intense than one of the species also present on silica–alumina cracking catalyst. These components resist outgassing at r.t. (Fig. 4b) and can be assigned to very strong, quasi-symmetrical hydrogen bonding, where the proton is partially but incompletely transferred to the base (Scheme 2, species III). This species gives rise to the so-called A, B (the features near 2950 and 2350 $cm^{-1}$ are called A and B components) or A, B, C contours (when a third component appears at even lower frequency) due to the Fermi resonance between the O-H stretching fundamental and the first overtones of the out-of-plane and in-plane O-H deformation modes of strongly interacting hydroxy groups. This phenomenon, well known in the field of fundamental IR spectroscopy, has been shown to occur on the surface of oxide materials for phosphate catalysts (56) and, more recently, it has been studied in detail for zeolites (57): on the other hand, the main band at 3602 $cm^{-1}$ fully disappears upon interaction with AN and outgassing.

The spectrum observed on HZSM5 in the presence of AN gas (Fig. 3a) is very different, and essentially presents extremely broad features. However, after outgassing at r.t. (Fig. 4a) the spectrum definitely changes and the ABC contour, with a very evident window at 2650 $cm^{-1}$ and apparent strong maxima at 2800 and 2450 $cm^{-1}$ (components

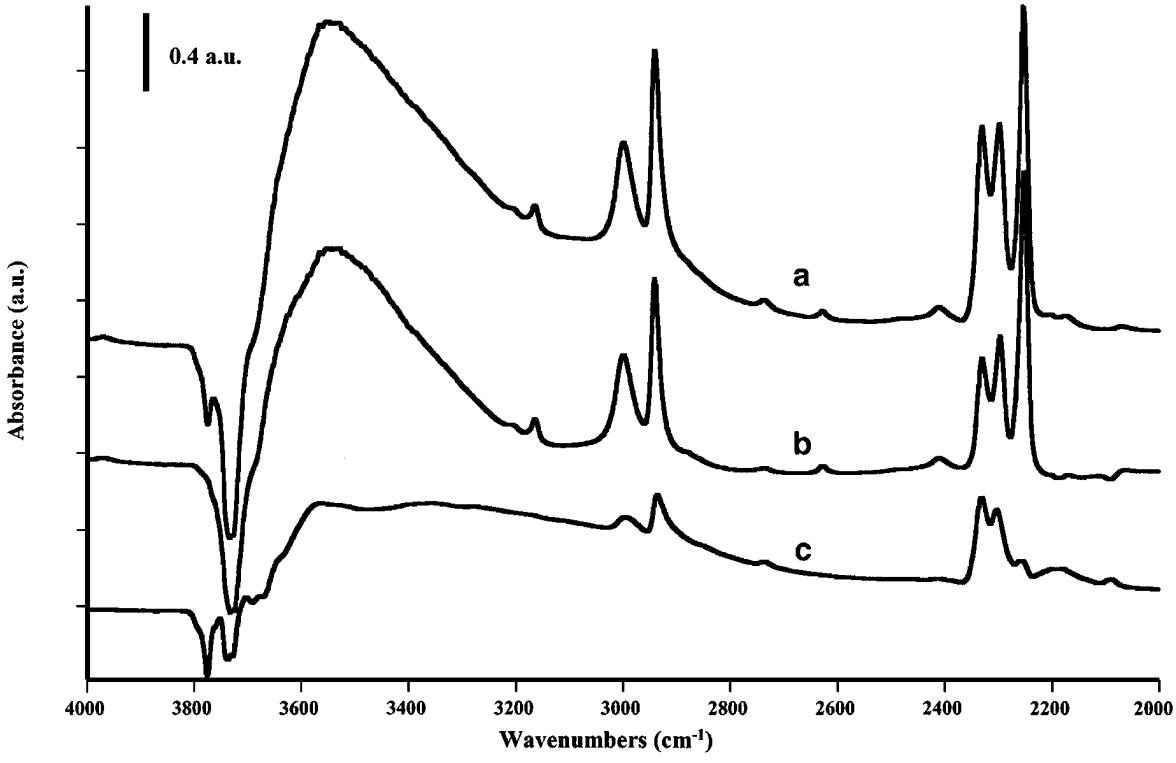


**FIG. 5.** Subtraction FT-IR spectra relative to adsorption of AN on AS: (a) upon contact with AN vapor (10 Torr) with the spectrum of the activated catalyst subtracted; (b) upon contact with AN vapor (10 Torr) and the spectrum of the outgassed catalyst subtracted; and (c) after outgassing at room temperature with the spectrum of the activated catalyst subtracted.

A and B, respectively, with a third one, C, that can be seen, weaker near 1630 $cm^{-1}$) appears. However, if we compare the position and the relative intensity of the A and B components in the spectrum recorded for HZSM5 and FER (both after outgassing, Figs. 4a and 4b) we note that the bands are shifted to lower frequencies in the former and the B component is stronger than the A component in the case of HZSM5 while the reverse occurs for FER. As described very well by Zecchina and co-workers (57), this means that the H-bonding of AN with Species III (Scheme 1) OHs is definitely stronger on HZSM5 than on FER. On the other hand, Species III (Scheme 1) is quite not detectable on HZSM5 in the presence of AN vapor (Fig. 3a). As will be discussed elsewhere (58), this is due to the formation of protonated dimeric species.

The data concerning the characterization of the Brønsted sites on these materials are summarized in Table 3.

### *(d) Interaction of Acetonitrile (AN) with the Surface Sites: Analysis of the vC≡N Modes*

In Fig. 6 the spectra of the adsorbed species arising from AN adsorption on the catalysts are also shown in the region 2450–2100 $cm^{-1}$. For each sample the upper spectrum is that recorded in contact with the gas (the gas-phase spectrum is subtracted) while the lower one was recorded after outgassing. In this region liquid acetonitrile shows a strong doublet at 2294, 2254 $cm^{-1}$, where the latter band is definitely stronger than the former. They are due to the Fermi resonance between the C≡N stretching and a $\delta CH_3 + \nu C{-}C$ combination (59).

For brevity, the results and the assignments are reported in Table 4. The spectra have been interpreted as due to the H-bonded species interacting with surface OHs and to species interacting with $Al^{3+}$ Lewis sites, according to the work of Krietenbrink *et al.* (60). The data fully agree with those reported above concerning H-bonding on OHs and show that on most of the above samples Lewis sites are present together with Brønsted sites. However, the strength of Lewis sites is apparently similar in all Al-containing samples except HZSM5, where Lewis sites are undetectable.

### *(e) Interaction of Pyridine (Py) with the Catalyst Surfaces*

The interaction of pyridine with the silica samples gives only rise to H-bonded species, desorbed upon outgassing, in agreement with the literature (30, 31). The spectrum of pyridine adsorbed on silicated alumina, AS, has been reported and discussed previously (7). Coordination on $Al^{3+}$ Lewis sites and H-bonding, mainly on silanol groups, was found, while no protonation occurs. The data arising from the interaction of pyridine and HZSM5 (Fig. 9b) are also

**TABLE 3**

**Summary of the Data on the Catalysts Brønsted Acidity**

| Catalyst | Notation | AN $\nu$OH | AN $\Delta\nu$OH | AN $T_{des}$ | Notes | Py | Assignments OH types |
|---|---|---|---|---|---|---|---|
| Pure silica | S1/S2 | 3746 | 300–330 | 300 | | H | I,II |
| Alumina | A | 3800–3600 | ca 200 | 300 | | H | Al-OH |
| Silicated alumina | AS | 3800–3600 | ca 200 | 300 | | H | Al-OH |
| | | 3730 | ca 200 | 300 | | H | IV |
| | | | ca 450 | 300 | | H | |
| Silica-alumina | SA13 | 3745 | = | 300 | | = | I,II unaccessible |
| | | 3740 | ca. 300 | 300 | | H | I,II |
| | | 3742 | ca 800 | 373 | | P | I' |
| Ferrierite | FER | 3745 | ABC | 373 | | P | I', external |
| | | 3602 | ABC | 373 | | = | III, internal |
| HZSM5 | HZSM5 | 3745 | ABC | 373 | | P | I', external |
| | | 3610 | ABC | 373 | pump | P | III, internal |
| | | | P | 300 | excess AN | | |

$T_{des}$ = Temperature for the desorption upon outgassing; H = hydrogen bonding;
P = protonation.

in agreement with previous data, showing predominant protonation to pyridinium ions and traces of coordination (43, 61).

The interaction of pyridine with silica–alumina at r.t. gives rise to the spectrum shown in Fig. 7a. The bands at 1597 and 1446 $cm^{-1}$ are due to the so-called 8a and 19b modes of pyridine molecules interacting via H-bonding with weakly acidic surface hydroxy groups, while the bands at 1623 and 1455 $cm^{-1}$ are due to the same modes of pyridine molecularly coordinated on $Al^{3+}$ cations, acting as Lewis acid sites.

The bands at 1639, 1547, and 1492 $cm^{-1}$ are the most intense modes of pyridinium cations, associated with a total proton transfer from the Brønsted acidic surface OH group to the basic molecule. According to these assignments, outgassing at 373 K (Fig. 7b) causes the disappearance of the bands at 1597 and 1446 $cm^{-1}$ (due to H-bonded pyridine), while the other, strongly held species are not perturbed. In Fig. 8 the spectra of the free surface OH groups on the silica alumina sample after activation and in the presence of adsorbed pyridine are shown. In these conditions we were able to resolve two components in the $\nu$OH band (Fig. 8a), the main sharp band at 3742 $cm^{-1}$ and an evident weaker maximum at 3746 $cm^{-1}$. In the conditions of Fig. 8b (i.e., after contact with pyridine vapor and outgassing at r.t.) the component at 3742 $cm^{-1}$ is almost completely disappeared, while a weaker and broad complex absorption with maxima near 3746, 3742, and 3735 $cm^{-1}$ are apparent. Outgassing at 373 K (Fig. 8c), causes only the very partial reappearance of a component near 3742 $cm^{-1}$, now only slightly more intense than the highest frequency component, observed at 3746 $cm^{-1}$. We mention that in these conditions H-bonded pyridine is disappeared but pyridinium ions are still present, unaffected. This implies that the "acid" OHs responsible for the pyridine protonation and the less acidic OHs involved for H-bonding are both responsible for the band near 3742 $cm^{-1}$. These data indicate that the band at ca. 3742 $cm^{-1}$ of silica–aluminas contains, in agreement with the data arising from AN adsorption and the conclusions of Rouxhet and co-workers (56, 55), the absorption of both weakly acidic species that H-bond pyridine (such as for silica) and strongly adsorbed species that protonate it. The species responsible for the component at 3745–3747 $cm^{-1}$ is either nonacidic or not accessible.

The spectrum of the species arising from pyridine adsorbed on FER is shown in Fig. 9a. The spectrum is clearly dominated by bands certainly due to pyridinium ions (1638, ca. 1610, 1544, and 1488 $cm^{-1}$), while the bands due to coordinated species (1622, 1455 $cm^{-1}$) are observed to be quite

**TABLE 4**

**Summary of the Data on the Catalysts Lewis Acidity**

| Catalyst | Notation | $\nu$C≡N Fermi resonance components | | Assignments |
|---|---|---|---|---|
| Liquid | | 2294 | 2254 | |
| Pure silica | S1/S2 | 2298 | 2265, 2255 | Weak H-bond |
| Alumina | A | 2298 | 2260 | Weak H-bond |
| | | 2335 | 2300 | Lewis site |
| Silicated alumina | AS | 2298 | 2260 | Weak H-bond |
| | | 2335 | 2300 | Lewis site |
| Silica-alumina | SA13 | 2298 | 2260 | Weak H-bond |
| | | 2335 | 2300 | Lewis site |
| | | | 2260 | Weak H-bond |
| Ferrierite | FER | 2305 | 2280 | Strong H-bond |
| | | 2335 | | Lewis site |
| HZSM5 | HZSM5 | 2309 | 2285 | Strong H-bond |

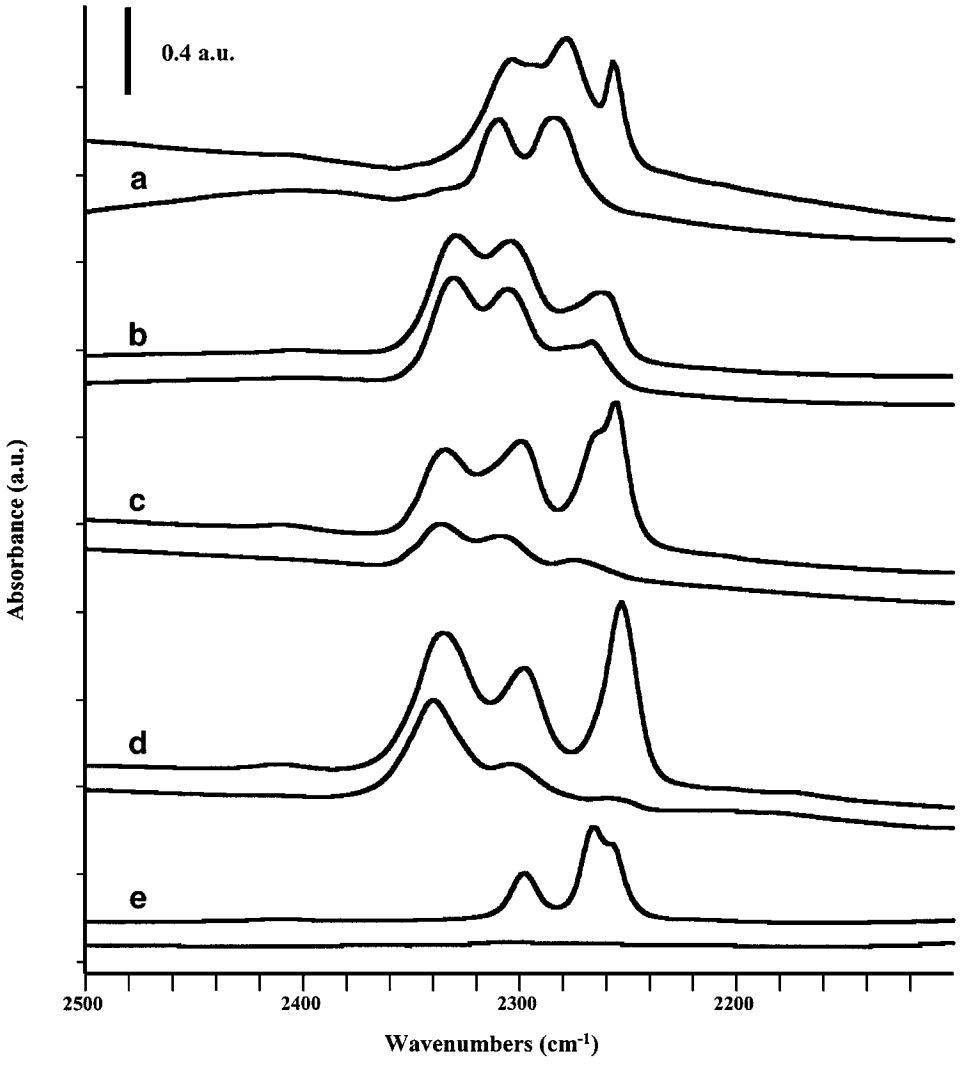


**FIG. 6.** FT-IR spectra in the C≡N stretching region of the adsorbed species arising from acetonitrile adsorption on the catalysts HZSM5 (a), FER1 (b), SA13 (c), AS (d), and S (e); for each catalyst, the upper spectra are recorded at 300 K in contact with the gas, the lower after further outgassing at 300 K.

weak. This spectrum is similar to that previously reported by Xu *et al.* (62). However, the simultaneous analysis of the O-H stretching region (Fig. 10a) shows that the OHs are almost unperturbed, after outgassing both at r.t. and at higher temperatures. The subtraction spectrum shows that pyridine adsorption on FER mainly perturbs the higher frequency $\nu$O-H band (3747 $cm^{-1}$) while it leaves the other IR bands unperturbed. Additional complex absorptions, possibly due to resonance of the N-H stretching of pyridinium with skeletal vibrations of the pyridine ring, are found in the range 3400–2800 $cm^{-1}$. These data suggest that pyridine could not enter the FER cavities, in agreement with their size, which does not allow the easy penetration of aromatics (43, 63). Thus, the pyridinium species are formed at the expense of external OHs, which are apparently characterized by the band at 3747 $cm^{-1}$, in spite of their strong Brønsted acidity.

## DISCUSSION

### *(a) Skeletal Isomerization and Nature of the Catalyst Acidity*

The data reported above show that the catalytic activity of materials belonging to the $SiO_2$–$Al_2O_3$ system in the conversion of *n*-butene could be correlated with the scale of their surface Brønsted acid strength, as determined by FT-IR spectroscopy of adsorbed acetonitrile and pyridine. In fact, from Tables 2 and 3, where the results on catalytic *n*-butene conversion and surface acidity characterization are summarized, the scale of both Brønsted acid strength and catalytic activity are A < AS < SA < FER < HZSM5. A different scale can be obtained for Lewis acidity, so that this further supports the idea that this reaction is Brønsted-catalyzed over all these catalysts.

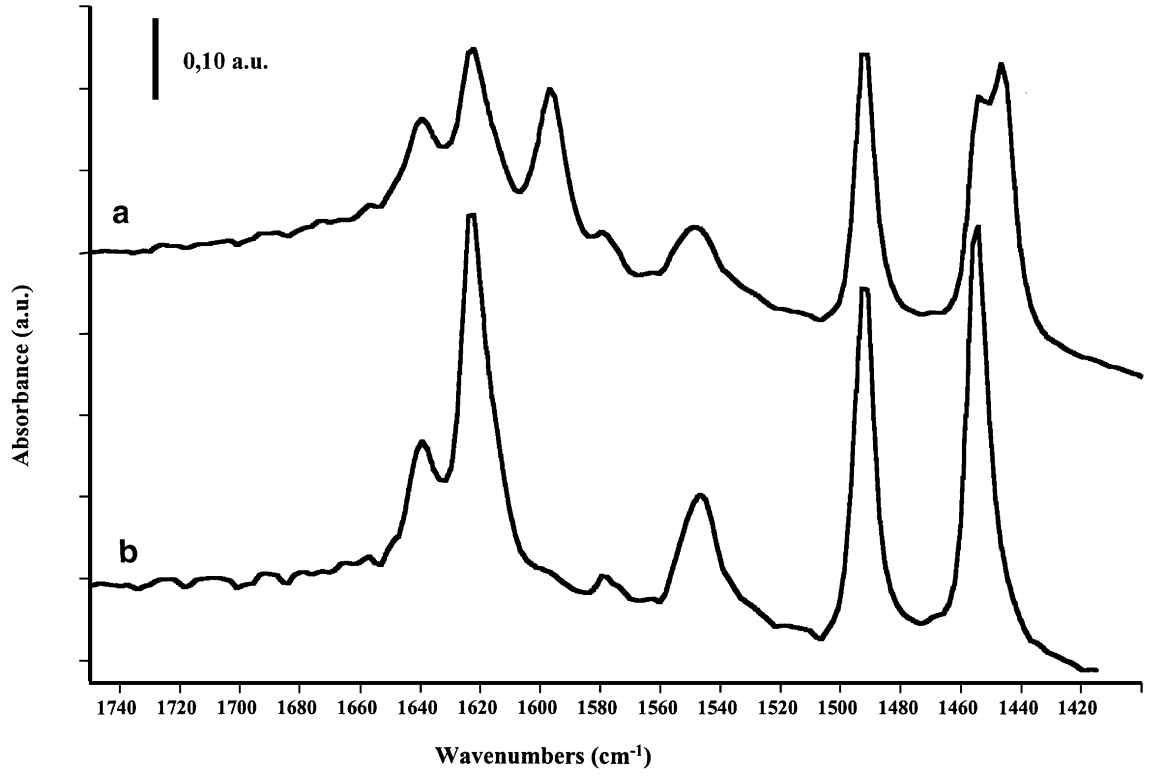


**FIG. 7.** FT-IR spectra of the surface species arising from adsorption of pyridine on a silica–alumina cracking catalyst (13% $Al_2O_3$, from Strem) at r.t. (a) and after outgassing at 373 K (b).

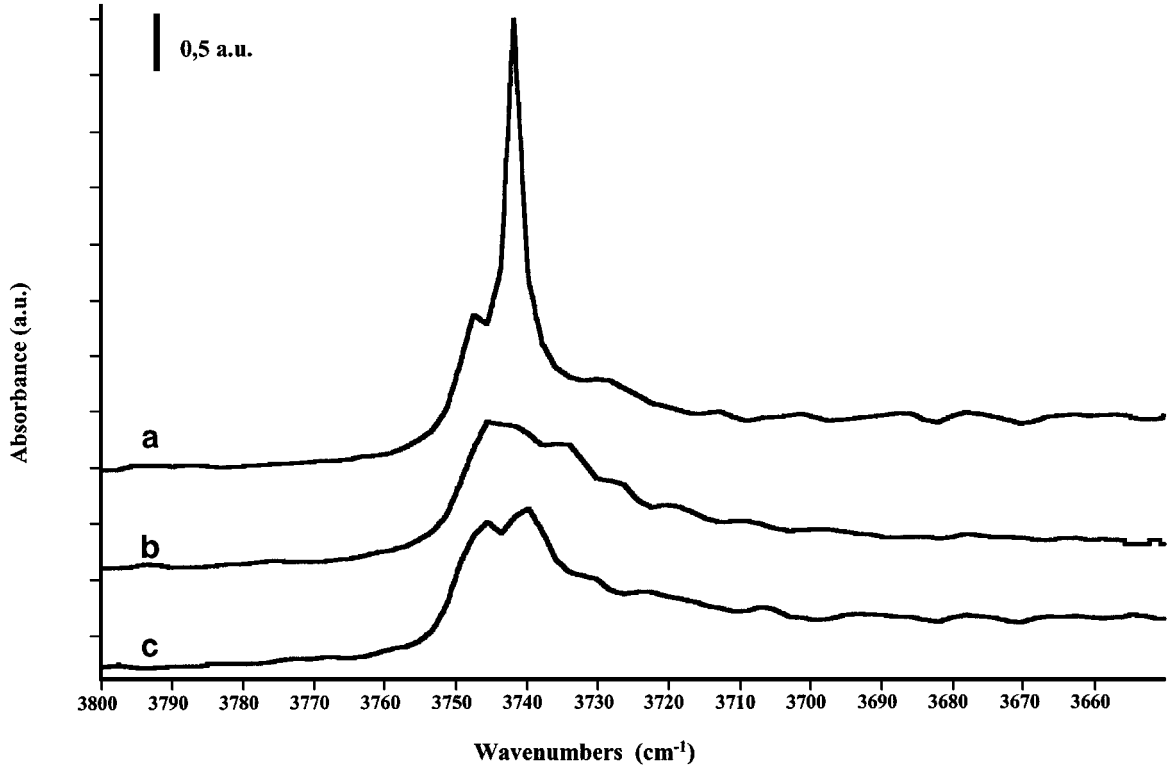


**FIG. 8.** FT-IR spectra of the surface hydroxy groups of a silica–alumina cracking catalyst (13% $Al_2O_3$, from Strem) after activation at 623 K (a), after contact with pyridine vapor and outgassing at r.t. (b), and after outgassing at 373 K (c).

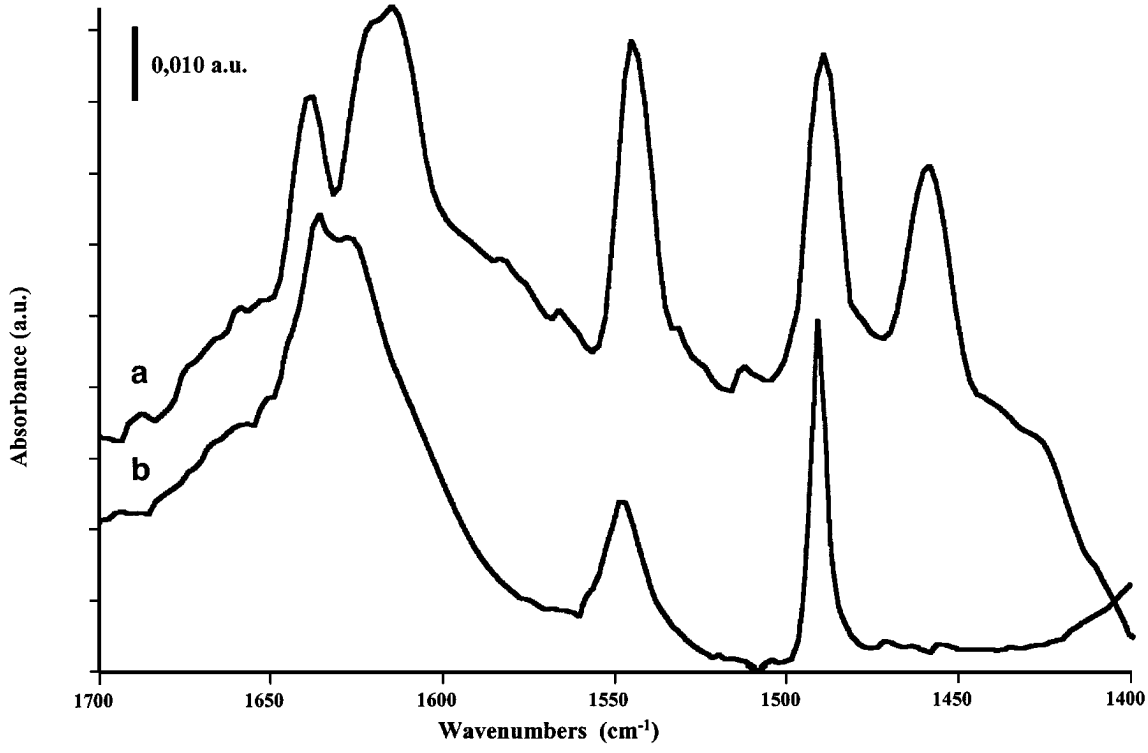


**FIG. 9.** FT-IR spectra of the adsorbed species arising from contact of FER1 (a) and HZSM5 (b) with Py vapor (3 Torr) and successive outgassing at 473 K.

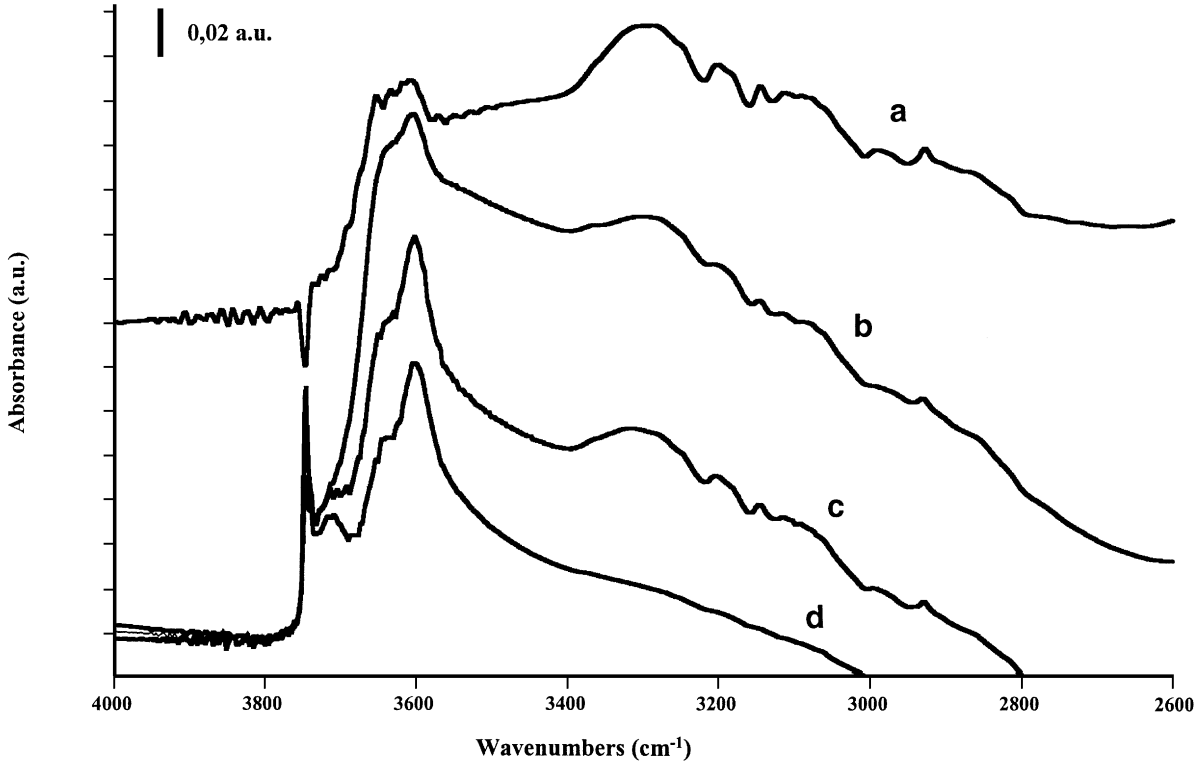


**FIG. 10.** FT-IR spectra of the surface hydroxy groups of FER1 after activation (a) and after contact with pyridine and successive outgassing at 373 K (b) and 473 K(c). (d) is the subtraction (c – a) showing the perturbation arising from pyridine adsorbed species still existing at 473 K.

This is not the same scale observed for other acid-catalyzed reactions. For example, in the case of methanol dehydration to dimethylether, recently Xu *et al.* (64) found the scale HZSM5 > A > SA in the absence of water. In fact, this reaction is known to occur with Lewis acid catalysis on aluminas (65) and with Brønsted-acid catalysis over zeolites.

### *(b) On the Structure of the Brønsted Acid Sites over Catalysts Belonging to the $SiO_2$–$Al_2O_3$ System*

The O-H stretching bands related to Si atoms can be found in two alternative regions. They can be alternatively located in the range 3748–3730 $cm^{-1}$, certainly due to terminal species (Scheme 1, Species I) and the other near 3600 $cm^{-1}$, typical of protonic zeolites and quite reliably assigned to bridging species like III (Scheme 1).

The data concerning adsorption of AN and Py and their interpretation support the following conclusions:

(i) The silanol groups of pure silica are terminal and interact weakly via H-bonding with both acetonitrile and pyridine.

(ii) The OHs on silica–alumina are also apparently all terminal (ca 3745 $cm^{-1}$) but they are clearly inhomogeneous, and comprehend at least two families of OHs, one of which interacts weakly and reversibly with both AN and Py and the other interacts strongly with AN and protonates pyridine.

(iii) The silanol groups on silicated alumina are again terminal. In spite of their lower O-H stretching frequency, most of them interact even more weakly with AN and Py than the OHs of silica. However, a fraction of more acidic OHs is likely also present on SA.

(iv) The external silanol groups of FER are essentially terminal, but they protonate pyridine.

(v) The internal OHs of FER and HZSM5 are bridging (ca 3600 $cm^{-1}$). They interact strongly by H-bonding with AN. In spite of the slightly higher O-H frequency, the internal OHs of HZSM5 are more acidic than those of FER.

(vi) Due to cavity size the internal OHs of FER are not available to large bases such as pyridine.

These data only partly agree with the previous literature. The existence of sites characterized by very similar O-H stretching frequencies but showing very different Brønsted acidities partly contradicts the current idea that the stronger is the Brønsted acid, the lower is its O-H stretching frequency. Actually, IR spectroscopists recognized long ago that the acidity versus O-H stretching function for even strongly related species is not monotonic (66). Also on surfaces, this is actually already known; as for example, it has previously been shown that preadsorption of ammonia on Lewis sites of some metal oxides decreases the acid strength of the surface OHs without shifting their frequency (67). This can be rationalized considering that the strength of a protonic acid is related to the difference between the free energies of it and of its conjugated base. On the contrary, the O-H stretching frequency is a property of the acid and does not takes into consideration the result of its dissociation.

Another current opinion that is not confirmed here is that the Brønsted acid sites on amorphous silica/alumina are similar to those in the zeolite cavities. In fact, the difference of their O-H frequencies strongly suggests that these sites are bridging in the zeolite cavities while are terminal in amorphous silica/alumina and in the external surface of FER.

The Brønsted acidity in zeolites (and on silica alumina too, following the literature) is considered to be related to the defect of cationic charge arising from the substitution of Al for Si in a silica-type framework, which is balanced by protons with are weakly linked to oxygen atoms, which are all bridging (Scheme 2, Species III).

A different scheme must justify the Brønsted acidity of the terminal silanols of silica-alumina (and of the external surface of FER). We suggest that also in this case, the insertion of aluminum cause the creation of a defect of charge. However, the bridge Si–OH–Al opens, due to the flexibility of the amorphous and/or external surface structure, giving rise to a terminal silanol and a Lewis acid site (Scheme 2, species I').

The formation of a bridging OH between a Si and an Al ion can be viewed as the result of a Lewis interaction between the "basic" oxygen of a terminal silanol and a Lewis acidic coordinatively unsaturated Al ion. However, the basicity of the oxygen of a Si–OH group is certainly very weak, according to the covalency of the Si-O bond. Thus, the silanol can prefer, when possible, to stand up in a terminal arrangement more than bridge over the Al Lewis site. When the proton is partly or totally transferred to a base, the silicate oxygen, now anionic, is definitely more basic, and can bridge easily over the Lewis acidic Al cation.

In this way, the presence of a near coordinatively unsaturated Al ion does not perturb significantly the silanol (which is still terminal) but stabilizes its dissociated forms (that becomes bridging), so increasing the absolute value of the negative $\Delta G$ of dissociation, i.e. increases the Brønsted acidity of the silanol.

The rigidity of the zeolite structures, instead, forces the OHs to stay bridging (Scheme 1, type III), also in the undissociated form further increasing their own free energy and, as a consequence, their acidity. At this point, its is still to be rationalized why the OHs of FER are less acidic than those of HZSM5. Moreover, the lower O-H stretching frequencies found for them, with respect to those of HZSM5 (3610 $cm^{-1}$), which look definitely more acidic, are to be justified.

### *(c) Brønsted Acidity Versus Skeletal Isomerization of Butenes*

These data can be interpreted with the reaction Scheme 3, already proposed by us for *n*-butene skeletal isomerization

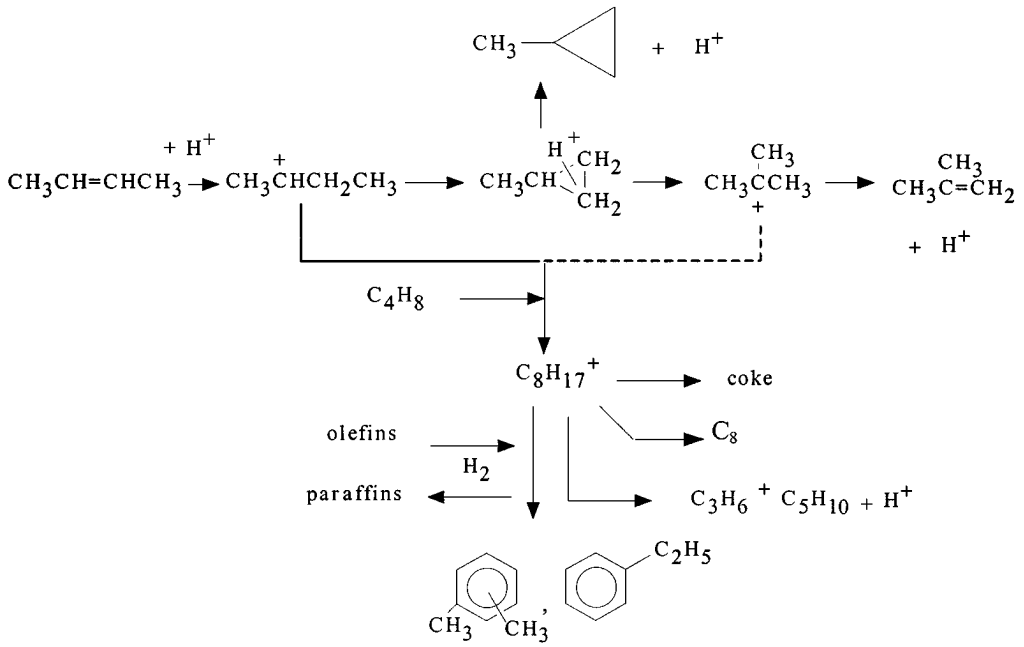


**SCHEME 3.** Reaction network for 2-butene skeletal isomerization based on the main product.

(7, 25), and apparently valid to interpret the reaction product distribution on all the materials investigated here.

According to Scheme 3, the reaction is catalyzed by the catalyst Brønsted acid sites, which protonate the *n*-butenes to produce the sec-butyl cation (detectable sometimes as an alkoxy group) that, through a protonated methylcyclopropane carbenium ion (12), gives rise, likely with a concerted mechanism (7, 25), to the tert-butyl carbenium ion. A proton elimination gives rise to isobutene, with a monomolecular mechanism, according also to Houzvicka *et al.* (2).

The hypothesis of a methylcyclopropyl carbocation-like transition state is supported by (i) the detection of traces (order of ppm) of methylcyclopropane as a reaction product, (ii) the detection of $C_2$-labeled *n*-butene starting from $C_1$-labeled *n*-butene after a short time on stream.

Dimerization to $C_8$ carbenium ions is apparently the main by-reaction in all cases. The evolution of the "$C_8$ surface pool" likely occurs via three main paths: (i) a "cracking mode" leading mainly to propene and a "$C_5$ surface pool," originating in the $C_5$ olefins, either linear and branched, whose distribution resembles the thermodynamic equilibrium, where at low conversion the ratio $C_3H_6/\Sigma C_5H_{10}$ is very close to unity; (ii) an "addition mode" to $C_{12}$ species; (iii) a "dehydrogenation mode" producing unsaturated compounds up to aromatics (xylenes are detectable in the product stream) and the so-called "coke." According to this scheme the main reaction (skeletal isomerization) and its main concurrent reaction (dimerization) start from a common intermediate (sec-butyl cation) and are Brønsted acid catalyzed. The selectivity is, consequently, determined mainly by the rates of the following steps. The elimination step from the tert-butyl carbenium ion to give isobutene can be assumed to be an acid–base reaction, needing a "basic" site on the catalyst surface to locate the proton. So this crucial step is certainly favored on weakly acidic catalysts carrying basic oxygens, more than on strongly acidic catalysts. This is the reason why, in our opinion, aluminas and alumina-based catalysts (which actually have an acido–basic character) allow high selectivities to isobutene.

In contrast, catalytic materials characterized by very covalent bonds lacking surface "basic" sites (such as silica, high-silica silica–aluminas, and HZSM5) do not assist such an elimination reaction, thus allowing dimerization to occur. On the other hand, dimerization is certainly favored by high butene pressures and low reaction temperatures. This is a further reason that very strongly acidic catalysts, which are very active in producing carbenium ions, do not allow good isobutene selectivity. In fact, although they can produce such ions at a low temperature also, in such conditions dimerization and oligomerization are favored.

The unusual properties of FER are certainly related to a shape selectivity effect. According to the above reaction scheme and after the works of Millini and Rossini (19) and of Houzvicka *et al.* (20), this effect should be related to the hindered formation of $C_8$ dimers into the FER pores, at least after some time on stream, i.e., after some coking (10, 16, 62) that would further limit the pore sizes. The hindering of the formation of $C_8$ dimeric carbenium ions is associated not only to the decreased formation of the $C_3 + C_5$ cracking products, but also to the decreased formation of aromatics and of alkanes, which are major products on very acidic catalysts such as HZSM5. The possibility of the formation of aromatics, in the absence of shape selectivity

effects, is very negative because the released hydrogen can react with butenes, converting them into butanes. This is what occurs on HZSM5 where isobutane, likely arising from successive hydrogenation of isobutene, is formed in big amounts. Thus, isobutene selectivity is also limited by a successive reaction, i.e., its hydrogenation. This is what occurs, according to Houzvicka *et al.* (20), in particular on high-Al-content HZSM5.

It must, however, be emphasized that other authors proposed a completely different reaction scheme, where FER would work with a bimolecular mechanism, with the dimer acting as an intermediate for isobutene formation (10, 18, 68, 69). However, Guisnet *et al.* (23) and Meriaudeau *et al.* (68) concluded, more recently, that the mechanism is bimolecular only during the fast initial coking, and becomes monomolecular after a few minutes on stream when the behavior is highly selective (as in our conditions).

On the other hand, the data reported here suggest that the good performances of FER can also be related to their acido–basic properties and possibly to complex distribution of its Brønsted acid sites. As discussed above, the high aluminum content gives rise to not so strongly acidic OHs and to the presence of more basic oxygen ions, which should be more useful for the production of isobutene.

Thus, an alternative hypothesis can be proposed to explain the positive effect of coking on selectivity to isobutene on FER. It is not excluded that coking kills the OHs that are still too acidic for isobutene synthesis, leaving those which allow skeletal isomerization to occur selectively. This hypothesis is, in our opinion, more satisfactory than the previous one, based on the limiting of the pore size by coke. In this case, in fact, a further progressive growth of coke would give rise first to a maximum in isobutene yield and later to a sudden stop of the isobutene production, when the pore size is reduced enough to allow skeletal isomerization and/or accessibility to pores. On the contrary, the data of Pellet *et al.* (11) show that FER samples (that after steaming and acid treatment have been freed by extraframework matter), show a very flat yield plateau even after extended pilot plant evaluation. According to Xu *et al.* (62) the coke formed on FER is aromatic and occupies only 11% of the FER micropores. This means that the OHs still present are not able to further produce coke. This definitely points to the presence of two different OH groups on FER with different (but not too high) acid strengths, one killed by coking and the other acting in catalysis.

The data reported above show that olefin skeletal isomerization catalysis is a medium strength acid catalysis reaction. It is evident that excessive acid strength favors by-reactions such as cracking, aromatization, and coking. However, shape selectivity effects, such as those observed on FER, can change the results, so that the best catalysts must be searched for among either medium-acid solids (aluminas) or shape-selective catalysts (FER). These two kinds of materials give quite comparable results in short-term experiments. However, stability to multiple reaction/regeneration cycles, resistance to impurities possibly present in the feeds, and low prices and availability are also required.

## CONCLUSIONS

The conclusions from the present results are the following:

(i) The surface Brønsted acid strength of catalysts belonging to the $SiO_2$–$Al_2O_3$ system, as studied through AN and Py adsorption, is the following: $SiO_2 < Al_2O_3 <$ silicated $Al_2O_3 < SiO_2$-$Al_2O_3 <$ FER < HZSM5.

(ii) The strongest Brønsted acidic hydroxy groups are terminal on $SiO_2$, $Al_2O_3$, silicated $Al_2O_3$, and $SiO_2$–$Al_2O_3$, while they are bridging on the zeolites FER and HZSM5.

(iii) On HZSM5, which carries the strongest Brønsted acidic hydroxy groups, protonation of acetonitrile to a dimeric cation and of pyridine is observed, while on $SiO_2$–$Al_2O_3$ and FER pyridine is protonated and acetonitrile is not. $SiO_2$, $Al_2O_3$ and silicated $Al_2O_3$ do not protonate either base.

(iv) The Brønsted acidity of the terminal OHs of $SiO_2$–$Al_2O_3$ is explained by the vicinity of coordinatively unsaturated Al cations, where after dissociation, the Si–$O^-$ group can bridge.

(v) The same scale is found for *n*-butene conversion, so that it is concluded, according to previous data, that this reaction is Brønsted acid catalyzed in all cases.

(vi) The scale of selectivities to isobutene is the reverse one, except for FER, which presents high selectivity.

(vii) The analysis of the by-products suggests that the main reaction consist in "monomolecular" skeletal carbenium ion isomerization, while the main by-reactions arise from dimerization of *n*-butene to $C_8$ dimeric carbenium ions.

(viii) The peculiar behaviour of coked FER is explained by a coexistence of a shape selectivity effect with the presence of residual medium-strength Brønsted acid sites.

## ACKNOWLEDGMENTS

Professor Blanka Wichterlová (Prague) is gratefully acknowledged for supplying a reference ferrierite sample.

## REFERENCES

1. Butler, A. C., and Nicolaides, C. P., *Catal. Today* **18**, 443 (1993).
2. Houzvicka, J., and Ponec, V., *Catal. Rev. Sci. Eng.* **39**, 319 (1997).
3. U.S. Clean Air Act Amendments. Public Law 101-549, November 15, 1990.
4. Raghavan, N. S., and Doraiswamy, L. K., *J. Catal.* **48**, 21 (1977).
5. Zheng, X. C., and Ponec, V., *J. Catal.* **148**, 607 (1994).
6. Buonomo, F., Fattore, V., and Notari, B., U.S. Patent 4013589, 1977; Buonomo, F., Fattore, V., and Notari, B., U.S. Patent 4013590, 1977; Manara, G., Fattore, V., and Notari, B., U.S. Patent 4038337, 1977.
7. Finocchio, E., Busca, G., Rossini, S. A., Cornaro, U., Piccoli, V., and Miglio, R., *Catal. Today* **33**, 335 (1997).

8. Miglio, R., and Cornaro, U., Eur. Patent EP667184 A1, 1995.
9. Catani, R., Cornaro, U., Miglio, R., Piccoli, V., Rossini, S., Finocchio, E., and Busca, G., *in* Proceedings, Intern. Symp., Acid–Base Catalysis III, Rolduc, Netherlands, 1997, No. O26.
10. Grandvallet, P., DeJong, K. P., Mooiweer, H. H., Kortbeek, A. G. T. G., and Kraushaar-Czarnetzki, B., Eur. Patent EP501577 (1992); Mooiweer, H. H., DeJong, K. P., Kraushaar-Czarnetzki, B., and Stork, W. H. J., *Stud. Surf. Sci. Catal.* **84**, 2327 (1994).
11. Pellet, R. J., Casey, D. G., Huang, H. M., Kessler, R. V., Kuhlman, E. J., O'Young, C. L., Sawicki, R. A., and Ugolini, J. R., *J. Catal.* **157**, 423 (1995).
12. Brouwer, D. M., and Hogeveen, H., *Prog. Phys. Org. Chem*. **9**, 179 (1972); Brouwer, D. M., *in* "Chemistry and Chemical Processes" (R. Prins and G. C. A. Schuit, Eds.), p. 137, Sythoff & Noordhoff, Rochville, MD, 1980.
13. Gates, B. C., "Catalytic Chemistry," Wiley, New York, 1992.
14. Olah, G. A., and Molnar, A., "Hydrocarbon Chemistry," Wiley, New York, 1995.
15. Seo, G., Jeong, H. S., Hong, S. B., and Uh, Y. S., *Catal. Lett.* **36**, 249 (1996).
16. Houzvicka, J., Klik, R., Kubelkova, L., and Ponec, V., *Appl. Catal. A Gen*. **150**, 101 (1997).
17. Guisnet, M., Andy, P., Gnep, N. S., Travers, C., and Benazzi, E., *J. Chem. Soc. Chem. Commun.*, 1685 (1995).
18. Guisnet, M., Andy, P., Gnep, N. S., Benazzi, E., and Travers, C., *J. Catal.* **158**, 551 (1996).
19. Millini, R., and Rossini, S., *in* "Progress in Zeolite and Microporous Materials" (H. Chon, S. K. Ihm, and Y. S. Uh, Eds.), p. 1389. Elsevier, Amsterdam, 1997.
20. Houzvicka, J., Hansildeer, S., and Ponec, V., *J. Catal.* **167**, 273 (1997).
21. Houzvicka, J., Diefenbach, O., and Ponec, V., *J. Catal.* **164**, 288 (1996); Houzvicka, J., and Ponec, V., *Ind. Eng. Chem. Res.* **36**, 1424 (1997).
22. Baeck, S. H., and Lee, W. Y., *Appl. Catal. A Gen*. **164**, 291 (1997).
23. Guisnet, M., Andy, P., Gnep, N. S., Travers, C., and Benazzi, E., *Ind. Eng. Chem. Res.* **37**, 300 (1998); Guisnet, M., Andy, P., Boucheffa, Y., Gnep, N. S., Travers, C., and Benazzi, E., *Catal. Lett.* **50**, 159 (1998).
24. Houzvicka, J., and Ponec, V., *Ind. Eng. Chem. Res.* **37**, 303 (1998).
25. Trombetta, M., Busca, G., Rossini, S., Piccoli, V., and Cornaro, U., *J. Catal.* **168**, 349 (1997).
26. Trombetta, M., Busca, G., Rossini, S., Piccoli, V., and Cornaro, U., *J. Catal.* **168**, 334 (1997).
27. Trombetta, M., Busca, G., and Willey, R. J., *J. Colloid Interface Sci.* **190**, 416 (1997).
28. Kilpatrick, J. E., Prosen, E. J., Pitzer, K. S., and Rossini, F. D., *J. Res. Natl. Bur. Stand*. **36**, 559 (1946).
29. Meriaudeau, P., Vu Anh, T., Le Ngoc, H., and Naccache, C., *in* "Progress in Zeolite and Microporous Materials" (H. Chon, S. K. Ihm, and Y. S. Uh, Eds.), p. 1373. Elsevier, Amsterdam, 1997.
30. Boehm, H. P., and Knözinger, H., *in* "Catalysis, Science and Technology" (J. R. Anderson and M. Boudart, Eds.), p. 39. Springer-Verlag, Berlin, 1983.
31. Morrow, B. A., *in* "Spectroscopic Characterization of Heterogeneous Catalysts, Part A: Methods of Surface Analysis" (J. L. G. Fierro, Ed.), p. 161. Elsevier, Amsterdam, 1990.
32. Hoffmann, P., and Knözinger, E., *Surface Sci.* **188**, 181 (1987).
33. Smirnov, K. S., *Vibrat. Spectrosc.* **4**, 255 (1993).
34. Morrow, B. A., and McFarlan, A. J., *J. Phys. Chem*. **96**, 1395 (1992).
35. Wojciechowski, B. W., and Corma, A., "Catalytic Cracking," Dekker, New York, 1986.
36. Corma, A., *Chem. Rev.* **95**, 559 (1995).
37. Busca, G., Lorenzelli, V., Ramis, G., and Willey, R. J., *Langmuir* **9**, 1492 (1993).
38. Morterra, C., and Magnacca, G., *Catal. Today* **27**, 497 (1996).
39. LiYi, Ramis, G., and Busca, G., *J. Mater. Chem*. **4**, 1755 (1994).
40. Quin, G., Zheng, L., Xie, Y., and Wu, C., *J. Catal.* **95**, 609 (1985).
41. Kustov, L. M., Kazansky, V. B., Beran, S., Kubelkova, L., and Jiru, P., *J. Phys. Chem*. **91**, 5247 (1987).
42. Zecchina, A., Bordiga, S., Spoto, G., Scarano, D., Petrini, G., Leofanti, G., Padovan, M., and Otero Arean, C., *J. Chem. Soc. Faraday Trans.* **88**, 2959 (1992).
43. Bhatia, S., Zeolite Catalysis: Principles and Applications, CRC Press, Boca Raton, FL, 1990.
44. Gajda, G. L., and Rabo, J. A., *in* "Acidity and Basicity of Solids: Theory, Assessment and Utility" (J. Fraissard and L. Petrakis, Eds.), NATO ASI series, p. 127. Kluwer Academic. Dordrecht, 1994.
45. Nicholas, J. B., *in* "11th Int. Congr. Catalysis—40th Anniversary" (J. W. Hightower *et al.*, Eds.), p. 1263. Elsevier, Amsterdam, 1996.
46. Astorino, E., Peri, J. B., Willey, R. J., and Busca, G., *J. Catal.* **157**, 482 (1995).
47. Jacobs, P. A., *Catal. Rev. Sci. Eng.* **24**, 415 (1982).
48. Naber, J. E., de Jong, K. P., Stark, W. H. J., Kuipers, H. P. C. E., and Post, M. F. M., Stud. Surf. Sci. & Catal. 84, *in* "Zeolites and related Microporous Materials; State of Art 1994" (J. Weitkamp *et al.*, Eds.), Studies in Surface Science and Catalysis, Vol. 84, p. 2197. Elsevier, Amsterdam, 1994.
49. Wichterlovà, B., Tvaruzkova, Z., Sobalik, Z., and Sarv, P., submitted for publication, personal communication.
50. Jin, Y. S., Auroux, A., and Vedrine, J. C., *Appl. Catal.* **37**, 1 (1988).
51. Komarov, V. S., and Malachevich, P. N., *Zh. Prikl. Spectrosk*. **37**, 7804 (1982).
52. Kunath, D., and Shulz, D., *J. Colloid Interface Sci.* **66**, 379 (1978).
53. Paukshtis, E. A., and Yurchenko, E. N., *Russ. Chem. Rev.* **52**, 426 (1983).
54. Sempels, R. E., and Rouxhet, P. G., *J. Colloids Interface Sci.* **55**, 263 (1976).
55. Scokart, P. O., and Rouxhet, P. G., *J. Colloids Interface Sci.* **80**, 96 (1982).
56. Ramis, G., Rossi, P. F., Busca, G., Lorenzelli, V., La Ginestra, A., and Patrono, P., *Langmuir* **5**, 917 (1989).
57. Zecchina, A., Bordiga, S., Spoto, G., Scarano, D., Spanò, G., and Geobaldo, F., *J. Chem. Soc. Faraday Trans.* **92**, 4863 (1996).
58. Trombetta, M., and Busca, G., submitted for publication.
59. Venkateswarlu, P., *J. Chem. Phys.* **19**, 293 (1951).
60. Krietenbrink, H., and Knözinger, E., *J. Chem. Soc. Faraday Trans. I* **72**, 2421 (1976).
61. Berndt, H., Lietz, G., Lucke, B., and Völter, J., *Appl. Catal. A Gen.* **146**, 1351 (1996); **155**, 121 (1997).
62. Xu, W. Q., Yin, Y.-G., Suib, S. L., and O'Young, C.-L., *J. Phys. Chem.* **99**, 758 (1995).
63. Ward, J. W., *in* "Applied Industrial Catalysis" (B. E. Leach, Ed.), Vol. 3, p. 272. Academic Press, New York, 1984.
64. Xu, M., Lunsford, J. H., Wayne Goodman, D., and Bhattacharyya, A., *Appl. Catal. A Gen*. **149**, 289 (1997).
65. Busca, G., *Catal. Today* **27**, 457 (1996).
66. Orville-Thomas, W. J., Galabov, B., Jalsovski, G., and Ratajczak, H., *J. Mol. Struct.* **19**, 761 (1973).
67. Hadjiivanov, K., Klissurski, D., Busca, G., and Lorenzelli, V., *J. Chem. Soc. Faraday Trans.* **87**, 175 (1991).
68. Meriaudeau, P., Bacaud, R., Ngoo Hang, L., and Vu, T. A., *J. Mol. Catal. A Chem*. **110**, L 177 (1996).
69. de Jong, K. P., Mooiweer, H. H., Bouglass, J. G., and Maarsen, P. K., *in* "Catalyst Deactivation 1997 "(C. H. Bartholomew and G. AS. Fuentes, Eds.), Stud. Surf. Sci. & Catal. **111**, p. 127. Elsevier, Amsterdam, 1994.